# Plasmonic Properties of Silver Trimers with Trigonal Symmetry Fabricated by Electron-Beam Lithography

**ARTICLE** *in* THE JOURNAL OF PHYSICAL CHEMISTRY C · AUGUST 2008

Impact Factor: 4.77 · DOI: 10.1021/jp804505k

# Plasmonic Properties of Silver Trimers with Trigonal Symmetry Fabricated by Electron-Beam Lithography

**Joan Alegret, Tomas Rindzevicius, Tavakol Pakizeh, Yury Alaverdyan, Linda Gunnarsson, and Mikael Käll***

*Applied Physics, Chalmers University of Technology, S-412 96 Göteborg, Sweden*

*Received: May 21, 2008; Revised Manuscript Received: July 3, 2008*

We investigate the dipolar plasmon modes of nanoparticle trimers formed by three equal silver disks of diameter $D = 100$ nm located on the vertexes of an equilateral triangle. Samples were fabricated by electron-beam lithography and studied experimentally by dark-field spectroscopy. The results are found to be in good agreement with electrodynamical simulations based on the discrete dipole approximation (DDA). Similar to nanoparticle dimers, the trimer system exhibits two hybridized dipole resonances to the red and to the blue of the single particle resonance. However, the far-field spectra are polarization-insensitive for light incident normal to the plane of the trimer, and the peak shifts, which occur as the edge-to-edge distance $d$ between the particles decrease, are smaller than for dimers. Moreover, we find that the dipolar displacement patterns are well described by linear combinations of bonding and antibonding symmetry adapted coordinates obtained through symmetry analysis based on the ideal $D_{3h}$ point-group.

## 1. Introduction

The recent decade has witnessed an enormous research effort directed toward understanding and utilizing the optical properties of metal nanostructures that support various types of plasmon resonances. This development of the "plasmonics" field[1] has been driven by the possibility of numerous exciting applications, including sensors,[2] metamaterials,[3] and nanophotonics components,[4] and enabled by the rapid progress in nanofabrication and computational electromagnetics. A particularly active subfield of plasmonics has been the study of near-field interactions between noble metal nanoparticles. The two most important consequences of such near-field coupling are, first, pronounced shifts of the plasmon resonance wavelengths compared to the single particle case, leading to a color change, and, second, a significant increase of local electromagnetic fields at interstitial sites between the particles. The first effect has, for example, been utilized in development of highly sensitive colorimetric detection schemes for DNA hybridization,[5] while the field-enhancement properties of interacting particles can, for example, be utilized for surface-enhanced Raman scattering.[6]

The great majority of experimental studies of plasmonic near-field coupling has focused on gold or silver particle dimers. Of particular interest are investigations of samples fabricated by electron beam lithography (EBL),[7−11] which enables nanometric control of the shape, size, and distance between particles. These studies have quantified the remarkable color changes that occur when two plasmonic particles approach each other: a red-shift, which may span a significant part of the visible spectrum, if the dimer is excited with light polarized along the dimer axis, and a much weaker blue shift for the perpendicular polarization configuration. The relative red-shift $\Delta\lambda_{LSP}/\lambda_{LSP}$, where $\lambda_{LSP}$ is the localized surface plasmon (LSP) resonance wavelength, is well approximated by an exponential decay $a \exp[-bd/D]$, where $d$ is the edge-to-edge separation between the particles, and $D$ is the particle diameter.[8,10,11] This "plasmon ruler" equation has recently been used to measure distances in biological systems separating plasmonic nanoparticles.[12,13]

In this contribution, we extend the dimer investigations to trimers composed of three equidistant silver disks. This trimer structure is interesting from a fundamental point-of-view because of the broken linear symmetry of the dimer and because the structure is the basic unit of a close-packed particle array, which is of high practical interest.[14,15] The plasmonic properties of arbitrary clusters of interacting spheres can, in principle, be obtained exactly using extended versions of Mie's theory; see ref 16 for an example of a trimer calculation, but such analytical solutions typically provide only limited physical insight into the resonant modes. In a recent report,[17] however, Brandl, Mirin, and Nordlander showed that the hybridized plasmon modes of trimers composed of point-like spheres could be constructed from group theory in a manner analogous to how linear combinations of atomic orbitals can be used to describe molecular orbitals.[18] We find that this description is valid also in the present case, despite the fact that the particles we investigate are discs with sizes that are not negligible compared to the resonance wavelength. As can be expected from previous dimer studies, we find considerable plasmon shifts as the distance between the particles decrease. However, the shifts are smaller than for dimers and do not follow the same "plasmon ruler" equation, thus highlighting the importance of the symmetry of the near-field plasmon interaction.

## 2. Materials and Methods

We prepared arrays of silver trimers consisting of three equidistant disks supported by a glass substrate using electron-beam lithography (EBL). A 70 nm thick electron-sensitive resist layer (ZEP520 diluted 1:2 in anisole) was first spin-coated on cleaned microscope cover slides. Prior to the exposure, a 10-nm gold film was thermally evaporated in a high-vacuum system (AVAC HVC 600) in order to avoid charging effects on the resist. The patterning was performed in a JEOL 9300 XS system, which has a minimum beam size of less than 5 nm. After the

* Corresponding author. E-mail: kall@chalmers.se.

10.1021/jp804505k CCC: $40.75 
Published on Web 08/26/2008

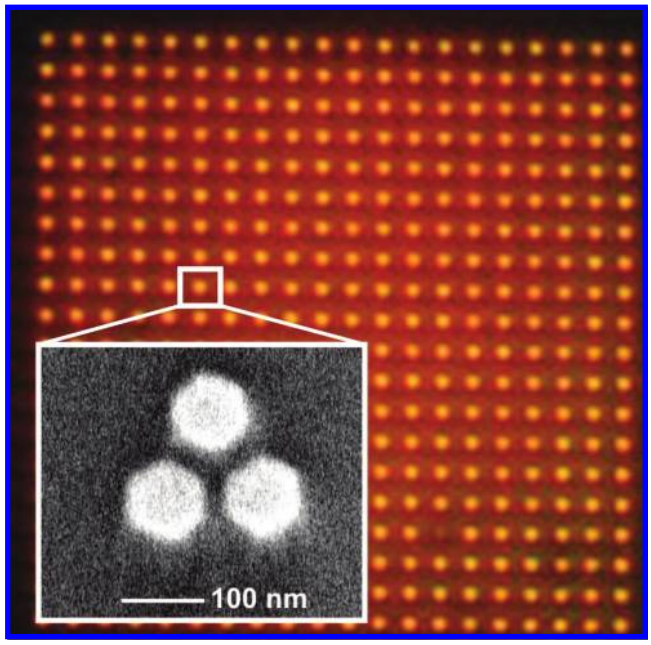


**Figure 1.** Dark-field microscopy image of an array of silver trimers on glass in immersion oil. Each red dot corresponds to one individual trimer composed of silver disks with diameter $D = 100$ nm and height $h = 25$ nm. This particular sample had an edge-to-edge distance $d = 20$ nm, while the lattice constant of the array is 1 $\mu$m. Inset shows a SEM image of one representative Ag trimer.

exposure, the 10-nm gold film was etched away in a solution of 4 g of KI and 1 g of $I_2$ in 150 mL of deionized water. The patterns were developed by dipping the samples in hexyl acetate for approximately 30 s, followed by rinsing in deionized water and drying in pure $N_2$ gas. An adhesion layer of 1 nm Ti and a silver film of the desired thickness were further deposited on the patterned resist. In the lift-off step, the remaining resist and the material on top of it were removed in acetone at 55 °C, followed by sequential rinsing in 2-propanol and deionized water and drying in pure $N_2$. The disks were made with a hexagonal base, which makes it easier to control the edge-to-edge separation than in the case of circular disks. The disk diameter was set to 100 nm and the height to 25 nm, and the edge-to-edge distance $d$ was varied between 10 and 500 nm. Each array consists of 400 trimers spaced 1 $\mu$m apart to reduce electromagnetic coupling between neighboring trimers. The disk separations and dimensions were determined using scanning electron microscopy (SEM) at low accelerating voltages. The inset in Figure 1 shows a typical SEM image of a trimer.

Optical characterization was performed through elastic scattering measurements in a dark-field (DF) microscopy setup, as described in ref 10. The samples were covered with immersion oil in order to obtain a uniform refractive index of $n = 1.51$ surrounding the nanostructures, which facilitate comparison between measured spectra and electrodynamics simulations. Elastic scattering spectra were collected with a fiber-coupled spectrometer. In order to ensure an efficient ensemble averaging within each array, we used a combination of magnification and fiber core thickness that produced a field-of-view covering a major part of each array. We present spectra obtained using s-polarized incident light, i.e. the incident field vector is oriented parallel to the sample substrate.

Simulations of far-field spectra and internal fields and polarizations were performed using the discrete dipole approximation (DDA) and the finite difference time domain (FDTD) methods. The DDA calculations were performed using

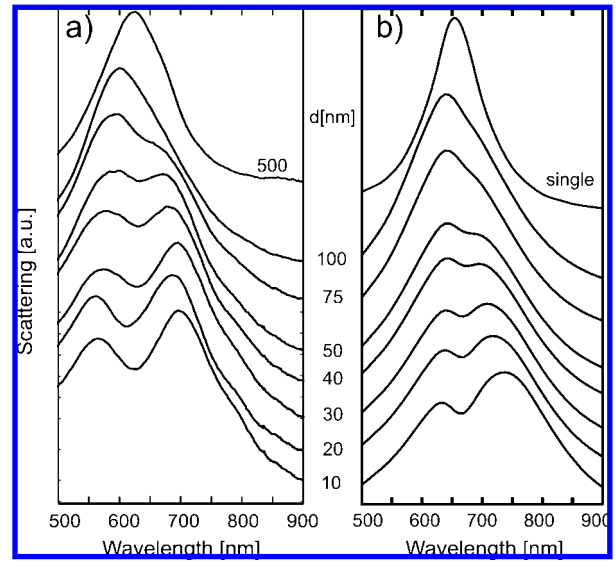


**Figure 2.** Experimental (a) and simulated (b) scattering spectra of Ag trimers for varying edge-to-edge distances $d$. The experimental data was obtained using s-polarized light with the incident k-vector aligned along the base of the trimers. The simulated spectra, obtained using the DDA technique, represent forward scattering, formally equivalent to extinction, for normal incidence but the same polarization as in the experimental case.

the open-source ADDA code,[19] modified so that experimental dielectric functions could be used. The mesh size was typically 2.5 nm, which corresponds to ~11000 dipoles in each particle. The dielectric function of silver was taken from ref 20. Dispersive FDTD calculations were performed as described in ref 21 using a mesh size of 3 nm. The experimental dielectric function, obtained from ref 22 was in this case fitted by a sum of four Lorentzian oscillators and a Drude term, which enable a facile transformation to the time-domain. The DDA and FDTD methods, in the implementations employed here, were found to yield nearly identical far-field spectra. The advantage of the former is that it gives access to internal polarizations/dipole orientations, while the latter enables simpler visualizations of electromagnetic near-fields.

## 3. Results and Discussion

Figure 2a shows experimental dark-field spectra for the Ag trimers as a function of the edge-to-edge separation $d$. The interaction between the particles is apparent from the considerable spectral changes that occur for decreasing separation: For $d = 500$ nm, corresponding to weakly interacting particles, we see a single peak at ~630 nm. The resonance position is in this case determined by the aspect ratio of the individual particles, and the peak corresponds to the dipolar LSP mode polarized parallel to the substrate plane.[10] However, already at $d = 75$ nm, one observes a clear splitting of the single particle mode. The long-wavelength peak, which is only seen as a flank on the main peak for $d = 100$ nm, is gradually red-shifting and increasing in strength until it dominates the spectrum for $d < 50$ nm. The remaining peak, in contrast, gradually decreases in intensity and exhibit a blue-shift.

The spectra in Figure 2a were measured with the incident polarization vector oriented normal to the base of the trimer (cf. Figure 1). However, rotating the polarization did not result in dramatic spectral changes. This is in marked contrast to the dimer case, for which polarization parallel to the dimer axis exclusively selects the red-shifted mode while perpendicular polarization singles out the blue-shifted resonance.[10]

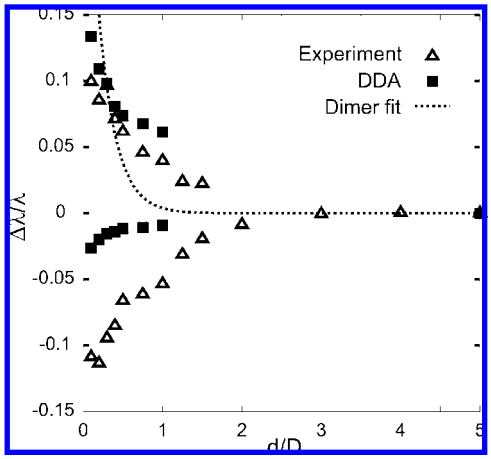


**Figure 3.** Relative shift in plasmon resonance wavelength versus scaling parameter *d/D* obtained from experimental trimer data (triangles) and DDA calculations (squares). The dashed line illustrates the corresponding variation for the long-wavelength plasmon of Ag dimers according to ref 10.

Figure 2b displays DDA results for trimers as a function of separation distance for the same polarization geometry as in the experiment. It is clear that these simulations capture the main features observed in the experiments, i.e. the splitting of the single particle plasmon and the gradual interchange of spectral weight between the two modes as $d$ decreases. In agreement with the experiments, the DDA simulations were also found to be independent of in-plane polarization. The differences between experimental and theoretical spectra are of the same magnitude as in many previous reports and are difficult to pinpoint. Possible causes for differences include slight deviations in particle shape, size, and separation between experiment and theory, errors in the dielectric function used for the simulations, differences in the excitation geometry (dark-field configuration vs normal incidence), and inhomogeneous broadening and weak long-range coupling[15] effects present in the experiment but not in the simulation.

It is interesting to compare the spectral shifts observed for the trimers to what has previously been reported for dimers composed of Ag particles of similar diameter $D$. Figure 3 summarizes the evolution of the relative trimer peak shifts $\Delta\lambda_{LSP}/\lambda_{LSP}$ as a function scaling parameter $x = d/D$. As a comparison, we have also included the "plasmon ruler" curve $\Delta\lambda_{LSP}/\lambda_{LSP} = a\exp[-bx]$, with $a = 0.37$ and $b = 0.22$, for the red-shifted dimer mode from ref 10. It is clear that there are substantial quantitative differences between the two systems: As mentioned above, the trimer exhibits a clear peak split already at large separations, of the order 10% at $d/D \approx 1$. To observe a similar peak split for the dimer, the separation has to decrease to $d/D \approx 0.5$.[10] At small separations, on the other hand, the dimer exhibits a larger peak split than the trimer, up to ~25% for the shortest particle separation investigated ($d/D = 0.105$) in ref 10 compared to ~20% for the trimer at $d/D = 0.1$. Also note that the latter effect results from the combination of a substantial blue-shift of the short-wavelength peak and a red-shift of the long-wavelength peak, whereas the peak split for the dimer almost exclusively results from a rapid red-shift of the long-wavelength peak at short separations.

In order to understand the spectral evolution described above, we utilize group theory. This methodology can be used to analyze plasmon modes in particle systems of well-defined spatial symmetry, see refs 23 and 24 for recent examples connected to metamaterials research. The trimers investigated here belong to the $D_{3h}$ point-group, characterized by a 3-fold rotation axis normal to the sample surface and vertical mirror symmetry due to the uniform refractive index surrounding the disks. As mentioned in the introduction, Brandl et al. thoroughly analyzed the case of three spheres with $D_{3h}$ symmetry.[17] Following that work, one can, using the projector operator technique, find an orthonormal basis set of dipolar displacements, so-called symmetry adapted coordinates (SACs), that constitute irreducible representations of the $D_{3h}$ point-group. There are a total of nine SACs, matching the original nine degenerate dipolar degrees-of-freedom of three independent particles. The SACs that correspond to in-plane displacements are shown in Figure 4 (the out-of plane modes are not considered further, as they are not excited in the experimental illumination configuration). As can be seen from Figure 4, the in-plane SACs fall into two classes: those with vanishing total dipole moment, i.e. the breathing (**B**) and rotation (**R**) SACs, and those with a finite moment. The latter belong to the E' representation of the $D_{3h}$ point group and are expected to dominate the optical response. As delineated in,[17] the E′ SACs are 2-fold degenerate: Referring to Figure 4, $\mathbf{X}_B$ and $\mathbf{Y}_B$ represent "bonding", or low-energy, combinations of the individual dipolar oscillations, while the $\mathbf{X}_{AB}$ and $\mathbf{Y}_{AB}$ SACs constitute antibonding, or high-energy, combinations. The energy of the different dipole combinations can be understood by analogy with the dimer case, i.e. an interaction mainly along the dipole orientation leads to a red-shifted/low-energy mode while an interaction mainly perpendicular to the dipole axis leads to a blue-shift/high energy. However, the two 2-fold degenerate real dipole-active normal modes of a trimer will always be a linear combination of the four E′ SACs.

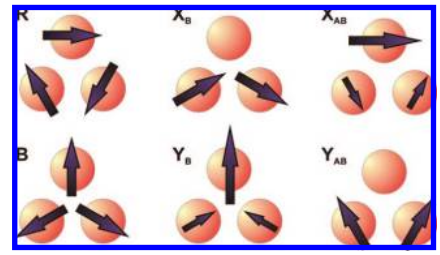


**Figure 4.** In-plane symmetry adapted coordinates (SACs) for dipolar modes in a trimer system with $D_{3h}$ symmetry. The six linearly independent SACs form an orthonormal system that can be used as a basis for an arbitrary combination of in-plane particle dipoles. "**B**" stands for the collective breathing-mode, "**R**" for the rotation mode, $\mathbf{X}_B/\mathbf{Y}_B$ for the bonding (low energy) modes polarized along $x/y$ and $\mathbf{X}_{AB}/\mathbf{Y}_{AB}$ stands for the corresponding antibonding (high energy) modes.

As an example, consider the case when the particles are far apart and illuminated with a plane wave polarized in the $y$-direction. With the $x$-axis in the horizontal direction in Figure 4 and defining the upper, lower left, and lower right particles as particle no. 1, 2, and 3, respectively, the dipole moments can be described as a vector $\mathbf{P} = [P_1^x\ P_1^y\ P_2^x\ P_2^y\ P_3^x\ P_3^y]^T$. Three noninteracting particles polarized in the $y$-direction can then be described as $\mathbf{P} = A^*[0\ 1/\sqrt{3}\ 0\ 1/\sqrt{3}\ 0\ 1/\sqrt{3}\ ]^T$, where $A = |A|e^{i\theta}$ is a wavelength dependent complex constant the magnitude of which determines the dipole strength and the phase of which refers to the phase shift in relation to the incident field (0 for wavelengths well to the red of the particle resonance and $\pi$ well to the blue). By projecting $\mathbf{P}$ on the SACs, one finds that $\mathbf{P} = A(a\mathbf{Y}_B + be^{i\varphi}\mathbf{Y}_{AB})$ with $\mathbf{Y}_B = 1/\sqrt{6}[0\ 2\ \sqrt{3}/2\ 1/2\ -\sqrt{3}/2\ 1/2\ ]^T$, $\mathbf{Y}_{AB} = 1/\sqrt{6}[0\ 0\ -\sqrt{3}/2\ 3/2\ \sqrt{3}/2\ 3/2\ ]^T$ and $a = b = 1/\sqrt{2}$, $\varphi = 0$. The bonding and antibonding SACs

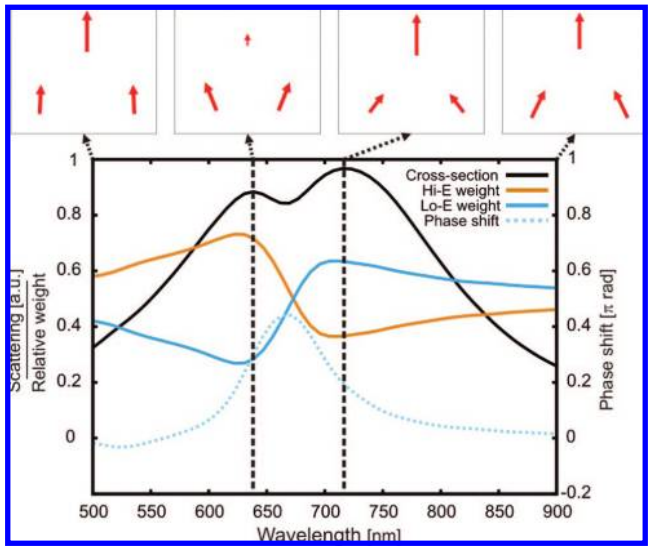


**Figure 5.** Particle dipole moments from DDA simulations and projection on SACs for an edge-to-edge separation of $d = 40$ nm. The upper four figures show trimer dipole moments obtained by summing all discrete dipoles from DDA simulations performed at the wavelengths marked in the extinction spectrum shown in the main figure, which also shows the contribution and relative phase shift between the $y$-polarized bonding and antibonding modes that build up the trimer dipole pattern.

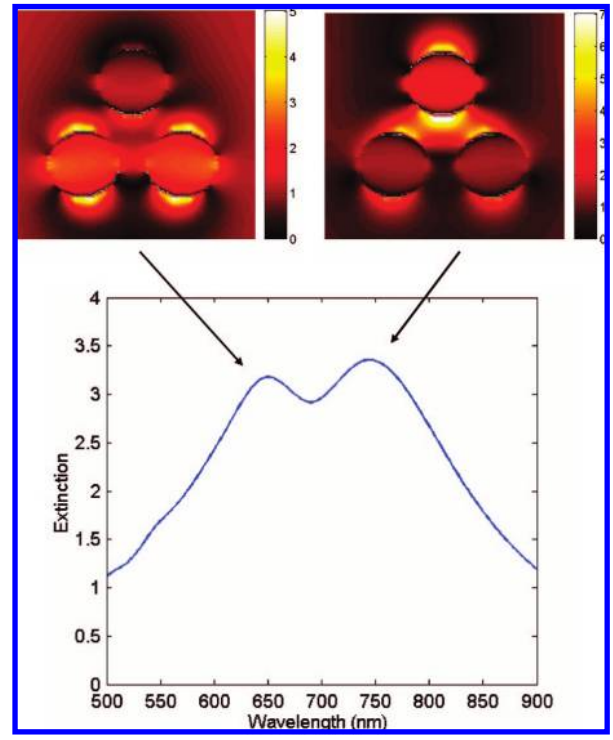


**Figure 6.** Electric field enhancement distributions obtained from FDTD simulation of a Ag trimer ($D = 100$ nm, $t = 20$ nm, $d = 40$ nm) in immersion oil ($n = 1.51$) at the peak wavelengths indicated in the accompanying extinction spectrum. The field plot is made in a plane 3 nm above the particle surfaces.

polarized in the $y$-direction thus contribute equally to the particle polarization at infinite separation, and there is no internal phase shift $\varphi$.

To understand the origin of the spectral peaks seen in the experimental data, we combined the symmetry analysis technique described above with the DDA calculations. The latter yield the elementary polarizations $\mathbf{p}(\mathbf{r})$ of all mesh elements within each trimer configuration as a function of wavelength. We sum the elementary polarizations for each particle and wavelength to obtain the corresponding total dipole moment components in the $x$- and $y$-directions, i.e. the vector $\mathbf{P}(\lambda)$. This is then projected on the different SACs. Figure 5 shows the results of this procedure for the case of a strongly interacting trimer ($d = 40$ nm) illuminated with $y$-polarized light. As expected, we find that only the $\mathbf{Y}_B$ and $\mathbf{Y}_{AB}$ SACs have non-negligible weights, i.e. the particle polarizations can be described as $\mathbf{P} = A(a\mathbf{Y}_B + be^{i\varphi}\mathbf{Y}_{AB})$ as above. However, the contribution of the two SACs, quantified as $a/(a + b)$ and $b/(a + b)$, respectively, varies strongly with wavelength, as does the relative phase shift $\varphi$.

Far from the resonances, i.e. at the end points of the spectral range displayed, one finds that the contributions from the two SACs gradually approach 50%, while the phase shift vanishes. The reason for this behavior is simply that the interaction between the particles decreases rapidly as one deviates from resonance, which means that the particle polarizations have to be the same as for three particles far away from each other, i.e. given by the polarization direction of the incident field. That this is the case can also be seen from the actual dipole orientations displayed at the top of the figure. Close to resonance, on the other hand, the contributions from the two SACs vary strongly with wavelength. Specifically, the long-wavelength peak is dominated by the low-energy bonding SAC $\mathbf{Y}_B$, while the high energy peak is dominated by the antibonding $\mathbf{Y}_{AB}$ SAC, as expected. This is also evident by comparing the particle polarization patterns corresponding to the two resonance positions, displayed at the top of the figure, with the displacement patterns of the two SACs shown in Figure 4. To further illustrate how the different particles contribute to each resonance, we show in Figure 6 FDTD simulations of the electric-field enhancement pattern. When the calculation is performed at the long-wavelength resonance, we see a pattern dominated by the dipolar near-field of the upper particle, while the two lower particles contribute weakly with dipole fields slightly inclined toward the center of the trimer. In the case of the short-wavelength resonance, the situation is reversed: the upper particle is almost dark and the field pattern is completely dominated by the two lower particles, which generates dipole fields inclined outward from the center of the trimer. These field patterns are thus fully consistent with the dipole oscillation patterns displayed in Figure 5.

With the dipole patterns discussed above in mind, we can return to the question of why the plasmon shifts as a function of separation are so different to the dimer case. We recall that the red-shifted dimer mode corresponds to an in-phase dipole oscillation parallel to the dipole axis while the weakly blue-shifted mode corresponds to an in-phase oscillation oriented perpendicular to the dimer axis. In the quasi-static point-dipole approximation of two particles of radius $a$ described by a Drude dielectric function, the frequency of these modes as a function of separation $d$ are $\omega_{LSP}\sqrt{1 - 2(a/d)^3}$ and $\omega_{LSP}\sqrt{1 + (a/d)^3}$, respectively, where $\omega_{LSP} = \omega_P/\sqrt{3}$ is the single particle resonance frequency (see for example ref 25). The former relation gives the physical background to the "plasmon ruler" dependence mentioned above. However, the dimer also supports two dipole forbidden normal modes that correspond to antiphase dipole oscillations parallel and perpendicular to the dimer axis. The energy of these modes are $\omega_{LSP}\sqrt{1 + 2(a/d)^3}$ and $\omega_{LSP}\sqrt{1 - (a/d)^3}$, respectively. From Figure 4, we see that the $\mathbf{Y}_B$ SAC is dominated by an in-phase dipole coupling along the $y$-axis that will cause a red-shift, but there is also a smaller antiphase

interaction in the *x*-direction from the two lower particles that will contribute a blue-shift. These competing effects qualitatively explain why the long-wavelength trimer mode exhibits a weaker red-shift as a function of separation than the dimer. Similarly, the $\mathbf{Y}_{AB}$ SAC can be thought of as two blue-shifting interactions that involve the two lower particles: an in-phase coupling perpendicular to the axis joining the two particles and an antiphase coupling parallel to this axis. Only the former, and weaker, of these contributions occur for a dimer, which may explain the larger blue-shift observed for the trimer.

Finally, one may note that we have not considered any multipolar modes in the preceding discussion. However, this does not mean that multipoles are unimportant. Multipolar fields contribute significantly to the coupling strength for small separations,[6,10,26] thus influencing the weights of the dipolar SACs at the two resonances, but their polarization contribution cancel out in the dipole sum leading to Figure 5. Likewise, their influences on the far-field spectra are small.

In summary, we have presented experimental and theoretical optical spectra of Ag particle trimers with trigonal symmetry. We find that DDA and FDTD simulations of this system can be interpreted in terms of a symmetry analysis based on simple point dipoles in the nonretarded limit according to Brandl et al.[17] Although experimental and theoretical spectra differ to some extent, we argue that this analysis must be valid also for the real plasmonic system under investigation. This is not *a priori* obvious, considering the fact that the overall size of the system ($\sim 2D + d \approx 200-300$ nm) is only about two times smaller than the resonance wavelength, which implies that retardation effects are not negligible. We further observe that the plasmon peak shifts that occur when the interparticle distances decrease are smaller than for the dimer case. This difference is qualitatively interpreted in terms of competing pairwise interactions within the trimer.

**Acknowledgment.** This work was supported by the Swedish Research Council and the Swedish Foundation for Strategic Research.

## References and Notes

(1) Atwater, H. A. *Sci. Am.* **2007**, *296*, 56.
(2) Lal, S.; Link, S.; Halas, N. J. *Nat. Photonics* **2007**, *1*, 641.
(3) Shalaev, V. M. *Nat. Photonics* **2007**, *1*, 41.
(4) Ozbay, E. *Science* **2006**, *311*, 189.
(5) Storhoff, J.; Elghanian, R.; Mucic, R.; Mirkin, C.; Letsinger, R. *J. Am. Chem. Soc.* **1998**, *120*, 1959.
(6) Xu, H. X.; Bjerneld, E. J.; Käll, M.; Börjesson, L. *Phys. Rev. Lett.* **1999**, 4357.
(7) Rechberger, W.; Hohenau, A.; Leitner, A.; Krenn, J. R.; Lamprecht, B.; Aussenegg, F. R. *Opt. Commun.* **2003**, *220*, 137.
(8) Su, K. H.; Wei, Q. H.; Zhang, X.; Mock, J. J.; Smith, D. R.; Schultz, S. *Nano Lett.* **2003**, *3*, 1087.
(9) Atay, T.; Song, J. H.; Nurmikko, A. V. *Nano Lett.* **2004**, *4*, 1627.
(10) Gunnarsson, L.; Rindzevicius, T.; Prikulis, J.; Kasemo, B.; Käll, M.; Zou, S.; Schatz, G. C. *J. Phys. Chem. B* **2005**, *109*, 1079.
(11) Jain, P. K.; Huang, W.; El-Sayed, M. A. *Nano Lett.* **2007**, *7*, 3227.
(12) Sonnichen, C.; Reinhard, B. M.; Liphardt, J.; Alivasatos, A. P. *Nat. Biotechnol.* **2005**, *5*, 2246.
(13) Reinhard, B. M.; Siu, M.; Agarwal, H.; Alivasatos, A. P.; Liphard, J. *Nano Lett.* **2005**, *5*, 2246.
(14) Gunnarsson, L.; Bjerneld, E. J.; Xu, H. X.; Petronis, S.; Kasemo, B.; Käll, M. *Appl. Phys. Lett.* **2001**, *78*, 802–804.
(15) Haynes, C. L.; McFarland, A. D.; Zhao, L.; Van Duyne, R. P.; Schatz, G. C.; Gunnarsson, L.; Prikulis, J.; Kasemo, B.; Käll, M. *J. Phys. Chem. B* **2003**, *107*, 7337–7342.
(16) Garcíade Abajo, F. J. *Phys. Rev. B* **1999**, *60*, 6086.
(17) Brandl, D. W.; Mirin, N. A.; Nordlander, P. *J. Phys. Chem. B* **2006**, *110*, 12302–12310.
(18) Cotton, F. A. *Chemical Applications of Group Theory*, 3rd ed.; Wiley-Interscience: New York, 1990.
(19) Yurkin, M. A.; Maltsev, V. P.; Hoekstra, A. *J. Quant. Spectrosc. Radiat. Transfer* **2007**, *106*, 546–557.
(20) Palik, E. *Handbook of optical constants of solids III*; Academic Press: San Diego, CA, 1998.
(21) Pakizeh, T.; Abrishamian, M. S.; Granpayeh, N.; Dimitriev, A.; Käll, M. *Optics Express* **2006**, *14*, 8240–8246.
(22) Johnson, P. B.; Christy, R. W. *Phys. Rev. B* **1972**, *6*, 4370.
(23) Urzhumov, Y. A.; Shvets, G.; Fan, J.; Capasso, F.; Brandl, D.; Nordlander, P. *Opt. Express* **2007**, *15*, 14129.
(24) Pakizeh, T.; Dmitriev, A.; Abrishamian, M. S.; Granpayeh, N.; Käll, M. *J. Opt. Soc. Am. B* **2008**, *25*, 659.
(25) Riikonen, S.; Romero, I.; García de Abajo, F. J. *Phys. Rev. B* **2005**, *71*, 235104.
(26) Romero, I.; Aizpurua, J.; Bryant, G. W.; García de Abajo, F. J. *Opt. Express* **2006**, *14*, 9988.

JP804505K